PHYSICAL REVIEW B **70**, 104427 (2004)

Structure and magnetic properties of the single-molecule magnet $[Mn_{11}CrO_{12}(O_2CCH_3)_{16}(H_2O)_4]\cdot 2CH_3COOH\cdot 4H_2O$: Magnetization manipulation and dipolar-biased tunneling in a $Mn_{11}Cr/Mn_{12}$ mixed crystal

Hidekazu Hachisuka and Kunio Awaga
Department of Chemistry, Graduate School of Science, Nagoya University, Chikusa-ku, Nagoya 464-8602, Japan

Toshihiko Yokoyama
Institute for Molecular Sciences, Okazaki 444-8585, Japan

Takeji Kubo
Nara University of Education, Nara 630-8528, Japan

Takao Goto
Graduate School of Human and Environmental Studies, Kyoto University, Yoshida, Sakyo-ku, Kyoto 606-8501, Japan

Hiroyuki Nojiri
Department of Physics, Faculty of Science, Okayama University, Okayama 700-8530, Japan

(Received 9 January 2004; revised manuscript received 3 May 2004; published 30 September 2004)

The structural and magnetic properties of the single-molecule magnet $[Mn_{11}CrO_{12}(O_2CCH_3)_{16}(H_2O)_4]\cdot 2CH_3COOH\cdot 4H_2O$ ($Mn_{11}Cr$) are studied through the analysis of a $Mn_{11}Cr/Mn_{12}$ ($\approx 1:1$) mixed crystal, where Mn_{12} is $[Mn_{12}O_{12}(O_2CCH_3)_{16}(H_2O)_4]\cdot 2CH_3COOH\cdot 4H_2O$. X-ray absorption spectra reveal that the Cr ion in $Mn_{11}Cr$ is in the +3 valence state and occupies a specific Mn^{3+} site in the Mn_{12} skeleton. High-frequency electron paramagnetic resonance (EPR) spectra are well explained by assuming that $Mn_{11}Cr$ is in a ground spin-state of $S=19/2$ with nearly the same EPR parameter set as for Mn_{12}. The lower spin quantum number results in lower barrier height (56.8 K) compared to Mn_{12}. The magnetization curves indicate a coercive field of 0.95 T for $Mn_{11}Cr$ at 1.8 K, nearly half that for Mn_{12}. Quantum tunneling of magnetization (QTM) in $Mn_{11}Cr$ is observed below the blocking temperature T_B, with the same field interval as for Mn_{12}. The magnetization of $Mn_{11}Cr$ and Mn_{12} in the mixed crystal can be independently manipulated by utilizing the difference between their coercive fields. The resonance fields of QTM in $Mn_{11}Cr$ are significantly affected by the magnetization direction of Mn_{12}, suggesting the effect of dipolar-biased tunneling.

DOI: 10.1103/PhysRevB.70.104427 PACS number(s): 75.50.Xx, 75.45.+j, 75.60.Ej

I. INTRODUCTION

The single-molecule magnet $[Mn_{12}O_{12}(O_2CCH_3)_{16}(H_2O)_4]\cdot 2CH_3COOH\cdot 4H_2O$ (hereafter Mn_{12}) possesses a high-spin ground state of $S=10$ due to antiferromagnetic interaction between the eight Mn^{3+} ($S=2$) ions and the four Mn^{4+} ($S=3/2$) ions in the cluster molecule.[1–3] The combination of this high spin multiplicity and strong uniaxial magnetic anisotropy (zero-field splitting constant D of ~ 0.6 K) results in an effective potential barrier between the up and down spin states.[2–4] At low temperatures, the magnetic moments do not rotate freely and the bistability associated with the uniaxial anisotropy results in a hysteresis loop in the magnetization curve.[4,5]

The simplified Hamiltonian for Mn_{12} is as follows:

$$\hat{H} = -DS_z{}^2 + g\mu_B SB + \hat{H}_1, \tag{1}$$

where D is the zero-field splitting, S_z is the z component of the spin operator, g is the g factor, and μ_B is the Bohr magneton. The second term describes the Zeeman energy associated with an applied field B, and the last term represents the transverse term, which brings about the quantum tunneling of magnetization (QTM) with a tunneling gap of ΔE.[6–8] The energy levels of positive and negative quantum numbers simultaneously cross at certain values of H_z, as given by

$$B_z \approx -\frac{Dn}{g\mu_B} \text{ with } n = 0,1,2,3,\ldots\ . \tag{2}$$

QTM in Mn_{12} is observed as a characteristic hysteresis loop in the magnetization curve, with small steps appearing at even intervals of the field.[6–8] It has been well established that QTM in Mn_{12} can be rationalized in terms of thermally assisted resonance tunneling, as QTM occurs effectively in thermally excited states.[9,10]

One of the outstanding features of molecular magnets is the ease of chemical modification. The physical phenomena of these materials can be readily understood by elucidating the effects of minor changes in the molecular skeleton, molecular packing, or electronic structure, amongst other properties.[11–19] The present study investigates the magnetic properties of $[Mn_{11}CrO_{12}(O_2CCH_3)_{16}(H_2O)_4]\cdot 2CH_3COOH\cdot 4H_2O$, having nearly the same molecular skeleton as Mn_{12} and a half-integer spin of $S=19/2$.

1098-0121/2004/70(10)/104427(7)/$22.50

II. EXPERIMENT

The mixed-metal cluster $\mathrm{Mn_{11}Cr}$ was prepared by reaction of $\mathrm{Mn(CH_3COO)_2 \cdot 4H_2O}$ with $\mathrm{K_2Cr_2O_7}$ at room temperature to afford mixed crystals of $\mathrm{Mn_{11}Cr}$ and $\mathrm{Mn_{12}}$.[12]

X-ray crystallography data was collected at room temperature using a four-circle diffractometer (MXC18K, MAC Science Co.). The structure was resolved by direct methods and Fourier techniques using MAXUS (MAC Science Co.).

K-edge x-ray absorption spectra for Cr and Mn were recorded at Beamline 9A in Institute of Materials Structure Science (Photon Factory, ring energy of 2.5 GeV and ring current of 400–250 mA) with a conventional transmission mode at room temperature. A Si(111) double crystal monochromator was employed and detuned by 40% to suppress higher-order harmonics. Both the incident and transmitted x-ray intensities were measured by ionization chambers filled with pure N_2. Cr 2*p* x-ray photoelectron spectra (XPS) were also recorded in laboratory using the VG ESCALAB 220i-XL system(a Mg $K\alpha$ source was used).

High-frequency electron paramagnetic resonance (EPR) measurements were performed by a simple transmission method. A conventional Gunn oscillator, Backward wave oscillator and an optically pumped far-infrared laser were employed as radiation sources, and InSb was used as a detector. Pulsed magnetic fields of up to 30 T were generated by a 100 kJ capacitor bank, at a pulse width of 8 ms. The details of the measurement system are described elsewhere.[20]

Dc and ac magnetic susceptibilities were recorded on a superconducting quantum interference device susceptometer (MPMS XL, Quantum Design). The angular-dependent magnetic properties were examined using a horizontal sample rotator.

III. RESULTS AND DISCUSSION

A. Molecular structure

Crystals of $\mathrm{Mn_{11}Cr}$* (* denotes mixed crystals of $\mathrm{Mn_{11}Cr}$ and $\mathrm{Mn_{12}}$) suitable for crystallographic analyses were grown by the method in the literature.[12] The chemical synthesis of pure $\mathrm{Mn_{11}Cr}$ was unsuccessful, and the ratio of the two cluster molecules in $\mathrm{Mn_{11}Cr}$* exhibited a weak batch dependence. X-ray crystal analyses were successful, and $\mathrm{Mn_{11}Cr}$* was concluded to have the same molecular structure and packing as $\mathrm{Mn_{12}}$. This suggests positional disorder of Cr in $\mathrm{Mn_{11}Cr}$*.

The extended x-ray absorption fine structure (EXAFS) functions of $k^3\chi(k)$ (k is the photoelectron wave number) were obtained by the standard procedures of pre-edge baseline subtraction, edge-energy determination, post-edge background subtraction (cubic spline), and normalization using the atomic absorption coefficients. Figure 1(a) depicts the $k^3\chi(k)$ functions for the experimentally obtained Cr (solid curve) and Mn (broken curve) absorptions. Fourier transforms of the $k^3\chi(k)$ functions (the k range is around 2.5–11.0 $\mathrm{Å^{-1}}$) are given in Fig. 1(b). While the Cr curve makes two peaks at 1.3 and 3.0 Å, the Mn curve makes three peaks at 1.3, 2.4, and 3.0 Å. The shortest distance (1.3 Å) is assignable to the O shells around Cr or Mn, and the other two shells at 2.4 and 3.0 Å are to those of Cr-Mn or Mn-Mn.

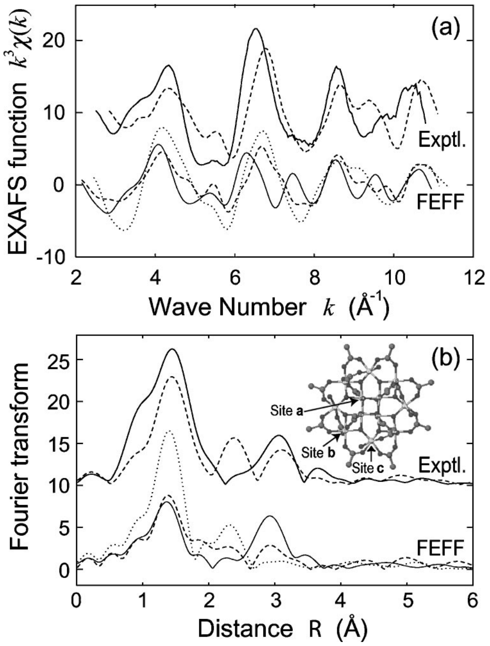

FIG. 1. (a) The Cr (solid curve) and Mn (broken curve) *K*-edge EXAFS functions $k^3\chi(k)$ of $\mathrm{Mn_{11}Cr}$*, together with the theoretical simulation results using FEFF8. The theoretical curves were obtained by assuming that Cr occupies site **a** (dotted curve), **b** (broken curve), or **c** (solid curve). (b) Fourier transforms of Fig. 1(a). The molecular structure is given in the inset, where sites **a**, **b**, and **c** are shown.

In Figs. 1(a) and 1(b), theoretical EXAFS functions are also shown. These results were obtained by performing the FEFF8 (Ref. 21) calculations of one $\mathrm{Mn_{11}Cr}$ molecule using the molecular structure determined in the present x-ray diffraction analysis. We have conducted three types of the calculations, where Cr occupies site **a** (dotted curve), **b** (dashed curve), or **c** (solid curve). See the inset of Fig. 1(b) for sites **a**, **b**, and **c**. Site **a** is occupied by $\mathrm{Mn^{4+}}$, while sites **b** and **c** are for $\mathrm{Mn^{3+}}$ in $\mathrm{Mn_{12}}$. The Fourier transform for the Mn absorption can be well understood as a superposition of the three theoretical curves in consistent with the fact that the Mn ions occupy the three sites. In other words, this justifies the present analytical procedure. In contrast, the Fourier transform for Cr is explained only by the theoretical one of site **c**. It is thus concluded that, in $\mathrm{Mn_{11}Cr}$*, $\mathrm{Cr^{3+}}$ occupies site **c**, the tilted site for $\mathrm{Mn^{3+}}$ in the $\mathrm{Mn_{12}}$ skeleton. The experimental Cr-O shell is much stronger than that of the theoretical one of site **c**. This is however easily understandable. The $\mathrm{Mn^{3+}}$ ion in site **c** exhibits significantly distorted octahedron due to the Jahn-Teller effect, resulting in the suppression of the Mn-O contribution. On the contrary, the $\mathrm{Cr^{3+}}$ ion shows no Jahn-Teller distortion, yielding more intense Cr-O contribution in the Fourier transform.

We have also measured Cr *K*-edge x-ray absorption near-edge structure (XANES) and Cr 2*p* XPS (figures not shown). The Cr $2p_{3/2}$ and $2p_{1/2}$ binding energies of $\mathrm{Mn_{11}Cr}$ were found to be exactly the same as those of $\mathrm{Cr_2O_3}$, and the Cr *K* edge energy in the XANES spectra of $\mathrm{Mn_{11}Cr}$ coincides with that of $\mathrm{Cr_2O_3}$. These findings are consistent with the above EXAFS results; the Cr ion in the $\mathrm{Mn_{11}Cr}$ cluster was consid-

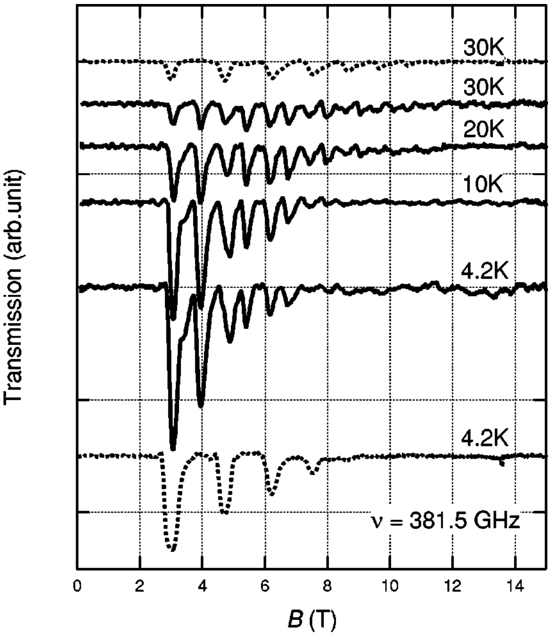

FIG. 2. High-frequency EPR (381.5 GHz) spectra for $\mathrm{Mn_{11}Cr^*}$ (solid curves) and $\mathrm{Mn_{12}}$ (broken curves) at various temperatures.

ered to be in the +3 state. Since octahedral $\mathrm{Cr^{3+}}$ ions are usually in the $S=3/2$ ground state, the ground spin state of $\mathrm{Mn_{11}Cr}$ is expected to be $S=19/2$. This will be confirmed by the high-frequency EPR, as shown in the next section.

B. High-frequency EPR spectroscopy

The results of high-frequency EPR (381.5 GHz) measurements on the crystals of $\mathrm{Mn_{11}Cr^*}$ are shown in Fig. 2. Spectra are shown for $\mathrm{Mn_{11}Cr^*}$ at 4.2, 10, 20, and 30 K, and $\mathrm{Mn_{12}}$ at 4.2 and 30 K. $\mathrm{Mn_{11}Cr^*}$ exhibits twice as many absorption lines as $\mathrm{Mn_{12}}$. The lowest-field absorption of $\mathrm{Mn_{11}Cr^*}$ (3.1 T) is in good agreement with that of $\mathrm{Mn_{12}}$. Regarding the second absorption (4.0 T), there is no corresponding one in the spectra for $\mathrm{Mn_{12}}$, but the third one agrees with the second-lowest-field absorption of $\mathrm{Mn_{12}}$. It is characteristic for $\mathrm{Mn_{11}Cr^*}$ that the odd-number absorption lines of $\mathrm{Mn_{11}Cr^*}$ are in agreement with the absorptions of $\mathrm{Mn_{12}}$ but there is no correspondence for the even-number absorptions. This feature can be interpreted by assuming that $\mathrm{Mn_{11}Cr^*}$ is a $\approx 1:1$ mixed crystal of $\mathrm{Mn_{11}Cr}$ ($S=19/2$) and $\mathrm{Mn_{12}}$ ($S=10$) with nearly the same EPR parameters. The resonance points for $\mathrm{Mn_{11}Cr^*}$ at the eight frequencies are shown in Fig. 3, where the closed and open circles are for the odd- and even-number absorptions, respectively. The solid lines show the theoretical ones calculated with the parameters for $\mathrm{Mn_{12}}$ ($S=10$) reported in Ref. 22: $g=1.96$; $D=-0.46\ \mathrm{cm^{-1}}$, $B_4^0=-2.2\times10^{-5}\ \mathrm{cm^{-1}}$, and $B_4^4=4\times10^{-5}\ \mathrm{cm^{-1}}$. They well explain the odd-number absorptions of $\mathrm{Mn_{11}Cr^*}$. The broken lines are, on the other hand, theoretical ones for the $S=19/2$ spin species with the same parameter set. The even-number absorptions of $\mathrm{Mn_{11}Cr^*}$ are well fit to the broken lines. EPR measurements indicate that there coexist $S=10$ and $19/2$ clusters with nearly identical anisotropy parameters. The former and latter can be ascribed to $\mathrm{Mn_{12}}$ and $\mathrm{Mn_{11}Cr}$, respectively, in the mixed crystals of $\mathrm{Mn_{11}Cr^*}$. The detailed EPR data will be published elsewhere.

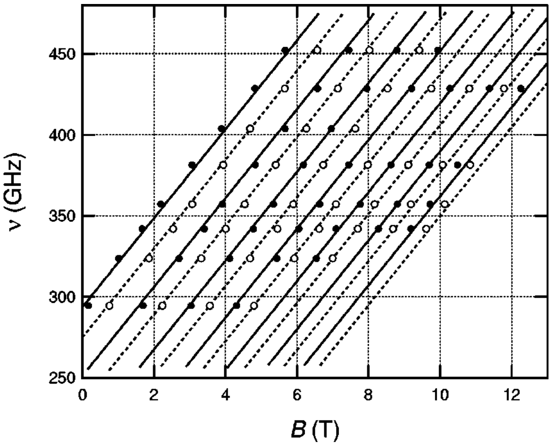

FIG. 3. The resonance points for $\mathrm{Mn_{11}Cr^*}$ at the eight frequencies. The closed and open circles indicate the positions of the odd-number and even-number absorptions, respectively. The solid and broken lines are theoretical ones for the $S=10$ and $S=19/2$ spin species, respectively, with the same parameter set (see the text).

EPR measurements indicated that $\mathrm{Mn_{11}Cr}$ has nearly the same parameter set as $\mathrm{Mn_{12}}$. This will be further supported by the angular-dependence measurements in Sec. III E. It is believed that the uniaxial anisotropy of $\mathrm{Mn_{12}}$ is caused by the Jahn-Teller distortions at the $\mathrm{Mn^{3+}}$ sites. Substitution of $\mathrm{Mn^{3+}}$ into non-Jahn-Teller $\mathrm{Cr^{3+}}$ is expected to bring about a significant change in the magnetic anisotropy, but this is not the case. It is hard to rationalize this with the present data, but let us suggest two possibilities. The EXAFS analyses revealed that $\mathrm{Cr^{3+}}$ occupies site **c** in the skeleton of $\mathrm{Mn_{12}}$. If the magnetic anisotropy of $\mathrm{Mn_{12}}$ is governed only by site **b** $\mathrm{Mn^{3+}}$, the replacement at site **c** would hardly affect the anisotropy. Another possible reason is a “template effect.” If the structure of $\mathrm{Mn_{11}Cr}$ is associated with the similar Jahn-Teller distortion as that of $\mathrm{Mn_{12}}$ in the solid state, making neighboring $\mathrm{Mn_{12}}$ molecules as a template, this may bring about similar anisotropy on $\mathrm{Mn_{11}Cr}$. There is a useful material, $[\mathrm{Mn_{12}}]^-$ ($S=19/2$), in which a site **c** $\mathrm{Mn^{3+}}$ is replaced with $\mathrm{Mn^{2+}}$.[23] Elucidation of this compound would bring about further information on the magnetic anisotropy of $\mathrm{Mn_{12}}$.

C. Magnetic susceptibility

The temperature dependence of dc and ac susceptibilities were examined in the ranges 1.8–300 K and 1.8–8 K, respectively. The temperature dependence of the dc susceptibilities for $\mathrm{Mn_{11}Cr^*}$ was nearly the same as that for $\mathrm{Mn_{12}}$. Figure 4 shows a comparison between the temperature dependence of the imaginary component of the ac susceptibilities χ'' for $\mathrm{Mn_{12}}$ (a) and $\mathrm{Mn_{11}Cr^*}$ (b). Data was obtained on polycrystalline samples in a zero-dc field and 2 Oe ac field at 10, 30, 99.9, and 250 Hz. The behavior of $\mathrm{Mn_{12}}$ is well known: χ'' exhibits a nearly symmetric peak with a systematic frequency dependence. In contrast, the χ'' peaks for $\mathrm{Mn_{11}Cr^*}$ have shoulders on the higher-temperature sides. Figure 4(c) shows the decomposition of the χ'' peak at 10 Hz

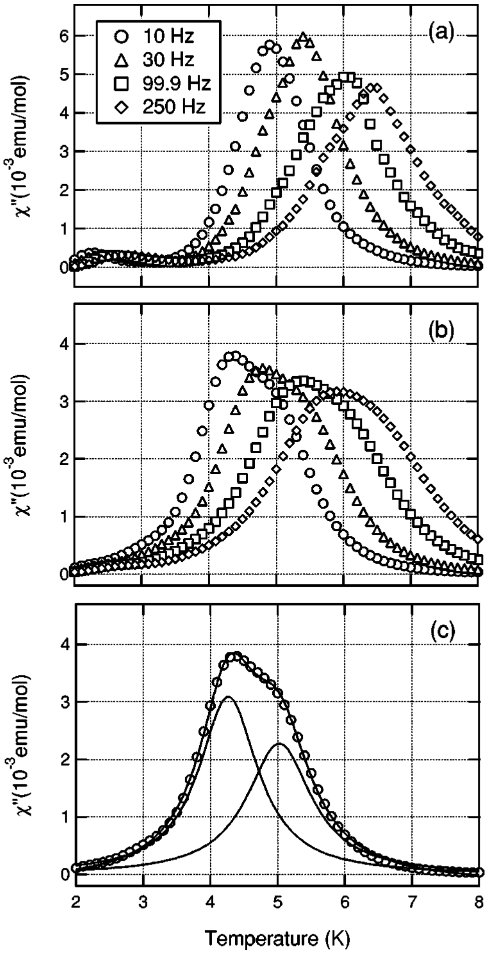

FIG. 4. Temperature dependence of ac magnetic susceptibilities for polycrystalline samples of (a) Mn_{12} and (b) $Mn_{11}Cr^*$ at various frequencies. The dependence for $Mn_{11}Cr^*$ (10 Hz) can be decomposed into two contributions (c).

into the two contributions; the solid curves show the components and their sum. The lower- and higher-temperature contributions are ascribable to $Mn_{11}Cr$ and Mn_{12}, respectively.

By decomposing the χ'' peaks of $Mn_{11}Cr^*$ into lower- and higher-temperature contributions, the temperature dependence of the relaxation time τ for $Mn_{11}Cr$ and Mn_{12} could be determined separately. Figure 5 shows Arrhenius plots for the two components, together with those for pure Mn_{12}. The obtained parameters are listed in Table I. The parameters for Mn_{12} in $Mn_{11}Cr^*$ are in agreement with those for pure Mn_{12}. The potential barrier in $Mn_{11}Cr$ is 56.8 K, which is lower than that for Mn_{12} by ≈20%. As the height of potential barrier is expressed by $\Delta E = DS^2$ and the D value for $Mn_{11}Cr$ is nearly identical to that of Mn_{12}, ΔE for $Mn_{11}Cr$ is expected to be lower than that for Mn_{12} by ≈10%. This small difference is attributed to a difference in tunneling relaxation in the thermally activated regime.[22,24]

D. Magnetization curve

The field dependence of dc magnetization was examined on one piece of crystal at 1.8 K in a field parallel to the easy axis (crystallographic *c* axis) at a sweeping rate of 0.17 mT/s. Figure 6 shows a comparison between the magnetization curves for Mn_{12} (a) and $Mn_{11}Cr^*$ (b). Both exhibit hysteresis loops with a stepwise change caused by QTM with nearly the same field interval of 0.475 T between the resonance fields. This is consistent with the fact that Mn_{12} and $Mn_{11}Cr$ possess nearly the same D value.[25–27] The lower graphs in Fig. 6 show the derivatives of the magnetization curves. While the dM/dB plots for Mn_{12} exhibit a maximum near the coercive field at which the magnetization changes the sign, the plots for $Mn_{11}Cr^*$ exhibit two high peaks at 0.95 and 1.775 T, the latter of which coincides with the largest peak for Mn_{12}.

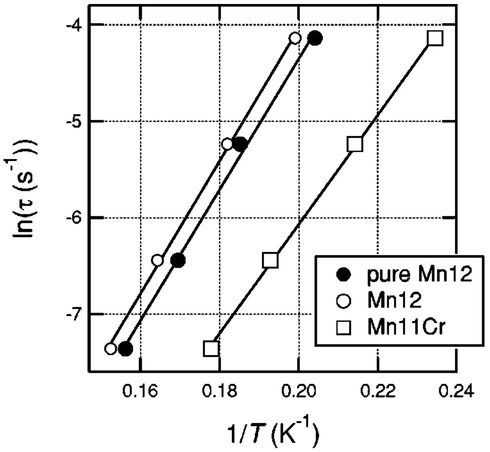

FIG. 5. Arrhenius plots of relaxation times τ obtained from the frequency dependence of the ac magnetic susceptibility. Open circles and squares denote the relaxations of Mn_{12} and $Mn_{11}Cr$ in $Mn_{11}Cr^*$, respectively. Closed circles represent the results for pure Mn_{12}.

According to the Kramers theorem,[28] no tunneling is allowed for half-integer spin systems in the zero field. However, there is no significant difference between the zero-field step-heights for Mn_{12} and $Mn_{11}Cr^*$. This could be explained by the fact that the zero-field step in this temperature range originates from fast-relaxation species of the Jahn-Teller isomers of Mn_{12}.[29,30]

To further understand the magnetization curve of $Mn_{11}Cr^*$, minor (or partial) loop measurements were conducted at 1.8 K, the results of which are shown in Fig. 7. The experimental conditions were the same as those employed for acquisition of the data in Fig. 6, except for the field-scan sequence. The sample was first cooled down below T_B under an applied field of 3.0 T to align the magnetizations of Mn_{12} and $Mn_{11}Cr$ in $Mn_{11}Cr^*$ parallel to the field. As the field was scanned from 3.0 to −1.2 T, the magnetization decreased to

TABLE I. Potential barriers ΔE, prefactors τ_0, and blocking temperatures T_B for $Mn_{11}Cr$ and Mn_{12}.

	$Mn_{11}Cr$	Mn_{12}
$\Delta E/k_B$ (K)	56.8	68.8
τ_0 (s)	2.8×10^{-8}	1.9×10^{-8}
T_B (K)	2.6	3.0

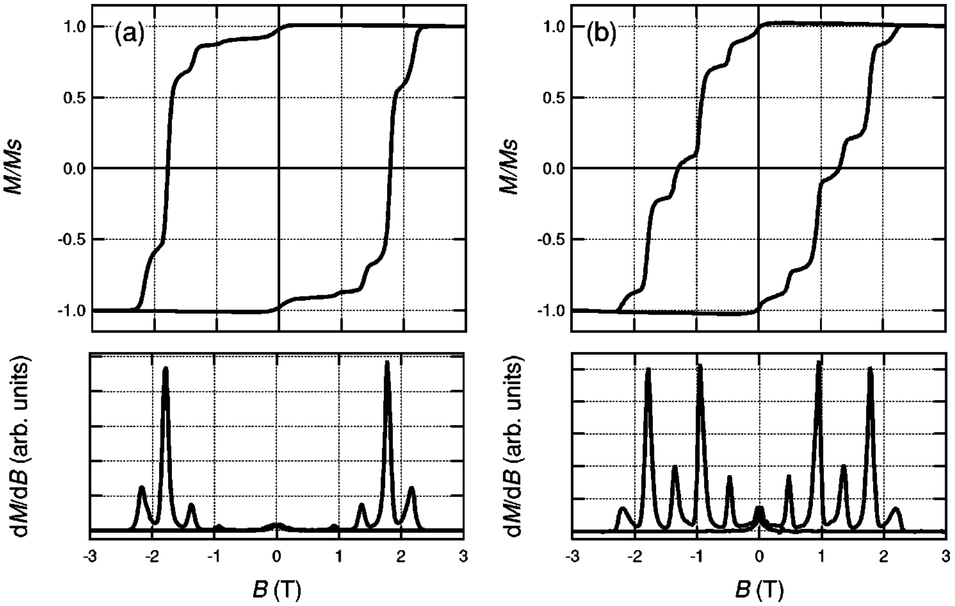

FIG. 6. Magnetization curves for Mn_{12} (a) and $Mn_{11}Cr^*$ (b) at 1.8 K at the sweeping rate 0.17 mT/s. The lower parts show the plots of dM/dB.

nearly zero via tunneling steps at −0.475 and −0.95 T. The field was then increased from −1.2 T to −0.2 T and back again. In this process, the magnetization was maintained constant, although entirely within a negative field. This means that the magnetization of half of the magnetic species in $Mn_{11}Cr^*$ was already relaxed toward the negative direction, whereas the other half was not affected by the negative field down to −1.2 T. As the field was scanned from −1.2 to −3.0 T, the magnetization decreased to the negative saturation value via two tunneling steps at −1.775 and −2.175 T. These measurements strongly indicate that the magnetization change in the field $|B| < 1.2$ T is caused by $Mn_{11}Cr$ with a coercive field of $B_c = 0.95$ T and the change in the field $|B| > 1.2$ T is due to Mn_{12} with $B_c = 1.775$ T.

The expected magnetization directions for Mn_{12} and $Mn_{11}Cr$ in the crystal of $Mn_{11}Cr^*$ are shown schematically in Fig. 7. Scanning the field in the order $-3.0 \rightarrow 1.2 \rightarrow 0.2 \rightarrow 1.2 \rightarrow 3.0$ T yield the same results. Therefore, it is concluded that the crystal of $Mn_{11}Cr^*$ stably stores the four spin structures formed by Mn_{12} and $Mn_{11}Cr$, switchable by means of an externally applied magnetic field.

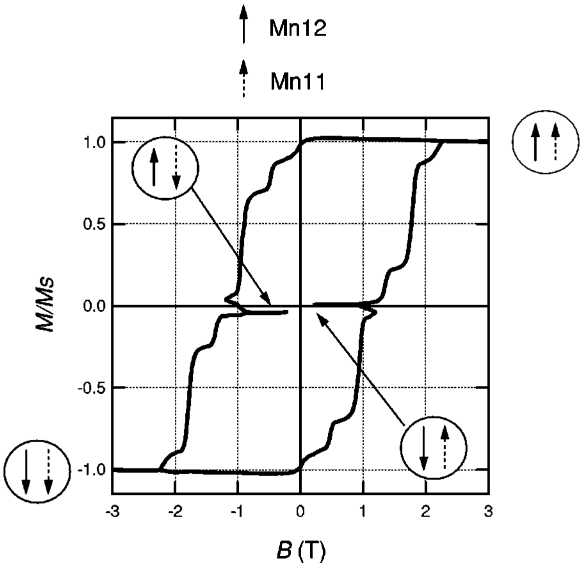

FIG. 7. Magnetization curves for $Mn_{11}Cr^*$ at 1.8 K showing the four stable states. Solid and broken arrows depict the directions of magnetization of Mn_{12} and $Mn_{11}Cr$, respectively.

In consideration of the observation that $Mn_{11}Cr^*$ involves two components with different B_c, another minor loop measurement was performed at 1.8 K. After annealing at 3.0 T, the field was scanned from 3.0 to −1.2 T, and then back to 3.0 T. The results are represented by the solid curve in Fig. 8(a). In the field 0−1.2 T, the two curves exhibit the magnetization changes of $Mn_{11}Cr$ from down to up via the tunneling process. However, a crucial difference can be observed in the direction of magnetization of Mn_{12}: it remains up, in contrast to the down exhibited by the full magnetization curve (broken line). Figure 8(b) shows the plots of dM/dB vs B for the two curves in the range 0−1.2 T. It can be clearly seen that the resonance peaks on the solid curve are shifted to lower fields by 0.05 T compared to the full magnetization curve, yet there is little difference in peak height. This is probably caused by a dipolar field produced by Mn_{12}; in the antiparallel configuration, this field adds to the applied field, so that the resonance field is reduced. On the contrary, in the parallel configuration the Lorentz field is opposite to the applied field, therefore increasing the effective resonance field to be applied to match the energy levels. The bias of the tunneling transitions is due to intermolecular couplings.

Exchange-biased tunneling was previously shown in a molecular dimer[31,32] and dipolar-biased tunneling was evidenced with mesoscopic Ho^{3+} ions.[33] The results obtained with $Mn_{11}Cr^*$ give another clear evidence of dipolar-biased tunneling, which can be tuned thanks to the stability of the parallel or antiparallel configurations in the relative orientation of the magnetization of $Mn_{11}Cr$ and Mn_{12} in $Mn_{11}Cr^*$.

E. Angular-dependent magnetic properties

The angular dependence of the magnetization curves for $Mn_{11}Cr^*$ was examined at 1.8 K on a plane that included the

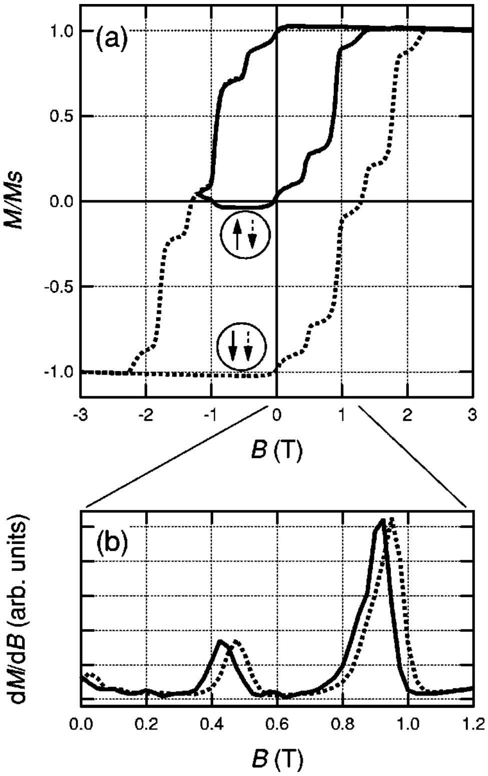

FIG. 8. (a) The full magnetization (broken curve) and minor loop measurement results (solid curve) for $Mn_{11}Cr^*$ at 1.8 K. (b) Plots of dM/dB in the range 0–1.2 T.

c axis. The results are shown in Fig. 9(a), where θ is the angle between the field and the axis. The sample was cooled from a temperature above T_B in a −3.0 T field, and measurements were taken as the field was increased to 3.0 T at 0.17 mT/s. The obtained magnetization curves clearly display the QTM steps with characteristic angular dependence. The QTM resonant fields are plotted in Fig. 9(b) as a function of θ. In case that the magnetic easy axes of Mn_{12} and $Mn_{11}Cr$ coincide with the respective molecular axes, the resonant fields for QTM between $|m\rangle$ and $|-m+n\rangle$ ($n=0,\pm1,\pm2,\ldots$) can be calculated as follows:

$$|B_n| = \left| n\frac{D}{g\mu_B \cos\theta} \right|. \tag{4}$$

The solid curves in Fig. 9(b) are the theoretical curves given by Eq. (4), and reproduce the angular dependence of the QTM in both $Mn_{11}Cr$ and Mn_{12} well. This means that the magnetic easy axes of both Mn_{12} and $Mn_{11}Cr$ are exactly parallel in a $Mn_{11}Cr^*$ single crystal. This is consistent with the results of the other magnetic measurements.

IV. CONCLUSIONS

The structural and magnetic properties of $Mn_{11}Cr^*$, an ≈1:1 mixed crystal of $Mn_{11}Cr$ and Mn_{12}, were examined in order to determine the structural and magnetic properties of $Mn_{11}Cr$. $Mn_{11}Cr$ includes Cr^{3+} at site **c** in the molecular skeleton of Mn_{12}, and has a spin quantum number of $S=19/2$. It was found that $Mn_{11}Cr$ has nearly the same D value and anisotropy as Mn_{12}. While the Jahn-Teller isomers of Mn_{12}, having different Jahn-Teller distortions at site **c**, exhibit quite different D values,[28] the introduction of non-Jahn-Teller Cr^{3+} ion into this site does not affect the magnetic parameters significantly. The four magnetization structures of $Mn_{11}Cr$ and Mn_{12}, namely, up-up, up-down, down-up, and down-down, were produced in the crystal of $Mn_{11}Cr^*$ as a result of the differences between the coercive fields of each of the constituents. Measurements of the QTM resonance field of $Mn_{11}Cr$ suggest the effect of dipolar-biased tunneling.

ACKNOWLEDGMENTS

The authors thank S. Miyashita and K. Takeda for helpful discussions. This work was supported in part by a Grant-in-Aid for Scientific Research from the Ministry of Education, Sports, Culture, Science and Technology (MEXT) of Japan. The XAFS measurements were performed under the approval of Photon Factory Program Advisory Committee (PF-PAC No. 2003G066). The XPS measurements were partly supported by "Nanotechnology Support Project" of MEXT.

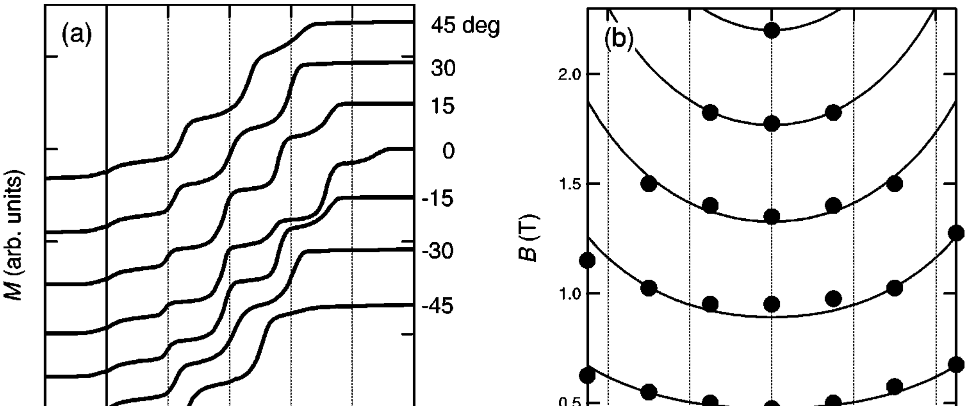

FIG. 9. Angular dependence of magnetization curves for (a) $Mn_{11}Cr^*$ at 1.8 K and (b) resonant fields for QTM. Solid curves represent the theoretical ones given by Eq. (4).

[1] T. Lis, Acta Crystallogr., Sect. B: Struct. Crystallogr. Cryst. Chem. **36**, 2042 (1980).

[2] A. Caneschi, D. Gatteschi, R. Sessoli, A. L. Barra, L. C. Bruel, and M. Guillot, J. Am. Chem. Soc. **113**, 5873 (1991).

[3] R. Sessoli, H.-L. Tsai, A. R. Schake, S. Wang, J. B. Vincent, K. Folting, D. Gatteschi, G. Christou, and D. N. Hendrickson, J. Am. Chem. Soc. **115**, 1804 (1993).

[4] H. J. Eppley, H.-L. Tsai, N. de Vries, K. Folting, G. Christou, and D. N. Hendrickson, J. Am. Chem. Soc. **117**, 301 (1995).

[5] R. Sessoli, D. Gatteschi, and M. A. Novak, Nature (London) **365**, 141 (1993).

[6] L. Thomas, F. Lionti, R. Ballou, D. Gatteschi, R. Sessoli, and B. Barbara, Nature (London) **383**, 145 (1996).

[7] J. M. Hernandez, X. X. Zhang, F. Luis, J. Bartolome, J. Tejada, and R. Ziolo, Europhys. Lett. **35**, 301 (1996).

[8] J. M. Hernandez, X. X. Zhang, F. Luis, J. Tejada, J. R. Friedman, M. P. Sarachik, and R. Ziolo, Phys. Rev. B **55**, 5858 (1997).

[9] J. R. Friedman, M. P. Sarachik, J. Tejada, and R. Ziolo, Phys. Rev. Lett. **76**, 3830 (1996).

[10] D. Gatteschi and R. Sessoli, Angew. Chem., Int. Ed. **42**, 268 (2003).

[11] A. R. Schake, H.-L. Tsai, N. D. Vries, R. J. Webb, K. Folting, D. N. Hendrickson, and G. Christou, J. Chem. Soc., Chem. Commun. **1992**, 181 (1992).

[12] Li Jin-Yu, Xu Hao, Zou Jian-Zhong, Xu Zheng, You Xiao-Zeng, and Yu Kai-Pei, Polyhedron **15**, 3325 (1996).

[13] K. Takeda and K. Awaga, Phys. Rev. B **56**, 14560 (1997).

[14] Y.-G. Wei, S.-W. Zhang, M.-C. Shao, and Y.-Q. Tang, Polyhedron **16**, 1471 (1997).

[15] D. Ruiz, Z. Sun, B. Albela, K. Folting, J. Ribas, G. Christou, and D. N. Hendrickson, Angew. Chem., Int. Ed. **37**, 300 (1998).

[16] Z. Sun, D. Ruiz, E. Rumberger, C. D. Incarvito, K. Folting, A. L. Rheingold, G. Christou, and D. N. Hendrickson, Inorg. Chem. **37**, 4758 (1998).

[17] P. Artus, C. Boskovic, J. Yoo, W. E. Streib, L.-C. Brunel, D. N. Hendrickson, and G. Christou, Inorg. Chem. **40**, 4199 (2001).

[18] C. Boskovic, M. Pink, J. C. Huffman, D. N. Hendrickson, and G. Christou, J. Am. Chem. Soc. **123**, 9914 (2001).

[19] M. Soler, W. Wernsdorfer, K. A. Abboud, J. C. Huffman, E. R. Davidson, D. N. Hendrickson, and G. Christou, J. Am. Chem. Soc. **125**, 3576 (2003).

[20] H. Nojiri, M. Motokawa, K. Okuda, H. Kageyama, Y. Ueda, and H. Tanaka, J. Phys. Soc. Jpn. **72**, 109 (2003).

[21] A. L. Ankudinov, B. Ravel, J. J. Rehr, and S. D. Conradson, Phys. Rev. B **58**, 7565 (1998).

[22] A. L. Barra, D. Gatteschi, and R. Sessoli, Phys. Rev. B **56**, 8192 (1997).

[23] S. M. J. Aubin, S. Spagna, H. H. Eppley, R. E. Sager, G. Christou, and D. N. Hendrickson, Chem. Commun. (Cambridge) **1998**, 803 (1998).

[24] F. Luis, J. Bartolome, J. F. Fernandez, J. Tejada, J. M. Hernandez, X. X. Zhang, and R. Ziolo, Phys. Rev. B **55**, 11448 (1997).

[25] S. M. J. Aubin, Z. M. Sun, H. J. Eppley, E. M. Rumberger, I. A. Guzei, K. Folting, P. K. Gantzel, A. L. Rheingold, G. Christou, and D. N. Hendrickson, Inorg. Chem. **40**, 2127 (2001).

[26] C. Boskovic, M. Pink, J. C. Huffman, D. N. Hendrickson, and G. Christou, J. Am. Chem. Soc. **123**, 9914 (2001).

[27] K. Takeda, K. Awaga, T. Inabe, A. Yamaguchi, H. Ishimoto, T. Tomita, H. Mitamura, T. Goto, N. Mori, and H. Nojiri, Phys. Rev. B **65**, 094424 (2002).

[28] H. A. Kramers, Proc. R. Acad. Sci. Amsterdam **33**, 959 (1930).

[29] K. Takeda, K. Awaga, T. Inabe, A. Yamaguchi, H. Ishimoto, T. Tomita, H. Mitamura, T. Goto, N. Mori, and H. Nojiri, Phys. Rev. B **65**, 094424 (2002).

[30] Y. Suzuki, K. Takeda, and K. Awaga, Phys. Rev. B **67**, 132402 (2003).

[31] W. Wernsdorfer, N. Aliaga-Alcalde, D. N. Hendrickson, and G. Christou, Nature (London) **416**, 406 (2002).

[32] B. Barbara, Nature (London) **421**, 32 (2003).

[33] R. Giraud, A. M. Tkachuk, and B. Barbara, Phys. Rev. Lett. **91**, 257204 (2003).